Proceedings of the ASME 2007 International Design Engineering Technical Conferences & Computers and Information in Engineering Conference
IDETC/CIE 2007
September 4-7, 2007, Las Vegas, Nevada, USA

DETC2007-34595

CABLE-SUSPENDED VEHICLE SIMULATION SYSTEM CONCEPT

Robert L. Williams II
Department of Mechanical Engineering
Ohio University, Athens, Ohio 45701
Email: williar4@ohio.edu

ABSTRACT

This paper presents a concept for virtual-reality-based vehicle simulation with whole-body haptics. The cable-suspended NIST RoboCrane is adapted to carry human operators in simulating a variety of vehicle motions. A realistic, immersive VR system is proposed with 3D graphics, haptic motion input devices, 3D surround-sound audio, articulating fans, and an olfactory generator. The real-world cockpit and input devices will be used to increase realism, suspended from nine active cables for motion simulation. The intent is to replace existing heavy, expensive, and dangerous Stewart-Platform-based flight simulators with a lighter, more economical, stiff, safe, high bandwidth, cable-suspended system. Many potential applications are proposed in addition to flight simulation. Our long-term goal is to create an economical, safe, realistic vehicle simulator with full-body motion for operator training, research & development, vehicle design, entertainment, rehabilitation, and therapy.

KEYWORDS

Vehicle simulation, cable-suspended robot, wire-driven system, whole-body haptics, workspace

1. INTRODUCTION

Flight simulation has been achieved using Stewart/Gough/Cappel-Platform-based octahedral hexapods (Stewart, 1965-66, Gough and Whitehall, 1962, and Cappel, 1967) since the 1960s (Bonev, 2003). These systems (for example, see Figure 1) have been proven to provide realistic flight simulations including transference of pilot training to real-world flight. However, they are too heavy, expensive, and dangerous for widespread application.

Parallel cable-suspended, or wire-driven, robots have been of great interest in the literature recently to enable robot systems with large workspace (at least translational), efficient actuation, extremely high payload-to-weight ratios, and other good potential characteristics. Pioneers in this area include the NIST RoboCrane (Albus et al., 1993) and the McDonnell-Douglas Charlotte robot (Campbell et al., 1995). Lafourcade et al. (2002) present a cable-suspended robot for posing small-scale aircraft models in wind tunnels.

The current paper presents a lighter, more economical, stiff, safe, high bandwidth, cable-suspended vehicle simulation system concept that has the potential to improve the Stewart Platform disadvantages (cost, size, safety) while expanding significantly the potential vehicle simulation applications. The current concept is intended for humans to ride and interact in various simulated vehicle dynamics situations. The main motion unit is an adapted NIST RoboCrane (Albus et al., 1993), which in itself is basically an inverted Stewart Platform with six stiff, lightweight active cables in place of the six hydraulic actuators. Actual cockpits from real-world vehicles, including the vehicle input devices (steering wheels, flight sticks, etc.) will be used to increase realism. A disadvantage of the proposed vehicle simulation system is that cables cannot push but can only apply tension; therefore, gravity and/or actuation redundancy is required to fully constrain the vehicle simulator motion.

Figure 1. Octahedral Hexapod F-16 Flight Simulator[1].

We herein propose many vehicles that can be simulated with immersion in VR, not just flight simulators. Since our system could be safer and much more economical, it could find widespread application in various missions that will be discussed. It is important to note that this is a concept paper; hence we do not yet attempt to prove any claims regarding improvements over the Stewart platform.

2. VEHICLE SIMULATION SYSTEM DESCRIPTION

Figure 2 presents the new concept for a Whole-Body Haptics Vehicle Simulator System (VSS). The 6-dof (*xyz* translations, *roll-pitch-yaw* rotations) motion for the human user is imparted using the

[1] www.mfg.mtu.edu/cyberman/machtool/machtool/altstruc/res5.html

ceiling-mounted six-cable-suspended robot. The rotations are rather limited, similar to a Stewart-Gough Platform, but the translational workspace can be quite large with a cable-suspended robot. Motors and cable reels are fixed to the ceiling and the cable ends are attached to the moving platform carrying the vehicle 'cockpit'. The system bandwidth and accelerations will be designed to allow a variety of vehicle simulations. The 'cockpit' is the real device from the real world, insofar as possible (see vehicle list given later), with real input devices for realism. We will include haptic (force-feedback) inputs where possible such as haptic flight sticks or haptic driving wheels. As shown in Figure 2, the cable robot is a modified NIST RoboCrane (Albus et al., 1993), which itself is a 3-3 Stewart-Gough platform inverted and hung from the ceiling, with active cables in place of hydraulic cylinder legs. We modify the RoboCrane to include three cables pulling down (see Figure 2) for crisp downward motions; that is, in this way we needn't rely on gravity for downward accelerations (plus, downward accelerations larger than g can be achieved in this manner). The down-pulling cables convert the gravity-constrained RoboCrane to a fully constrained cable robot. Figure 2 also shows a passive gravity off-load system that will be designed to partially relieve the weight due to gravity, allowing smaller motors for the same desired accelerations in motion. Not shown, there will have to be redundant safety systems developed to ensure human passenger safety during all vehicle motion simulations.

We envision two control modes for vehicle simulation: 1. Pre-programmed, 'canned' motion of the vehicle in which a human can ride passively to experience the simulated dynamics; and 2. Active, real-time mode wherein the human 'pilot' enters vehicle motion commands through realistic control inputs and experiences the dynamics of his or her commands in the resulting simulated motions. Dynamics and control are not presented in the current paper.

Below we discuss the possible vehicles, system components, and possible applications of this proposed vehicle simulation system.

2.1 Range of Possible Vehicles for Simulation

This vehicle simulation system concept allows for a large variety of real-world vehicles to be simulated, with their real-world cockpit physically suspended from the nine active cables for the human user to ride in, including, but not limited to, the following:

- Aircraft, Gliders, Hang Gliders, Dreamtime 'Peter Pan' Flight
- Automobiles, Motorcycles, Four-wheelers, Snow-mobiles, Tractors
- Sailboats, Windsurfers, Kayaks, Jet Skis
- Mountain Bikes, Skateboards, Downhill and Cross-country skiing
- Equestrian riding
- Roller Coasters and other Thrill Rides

The same system could be quickly modified to allow various real-world cockpits to be interchanged as desired in the same laboratory, clinic, or arcade. Thus, one cable-suspended robot and VR system could handle many different needs.

Even given a specific type of vehicle, such as automobiles, different options may be programmed and presented to the user for a choice to represent different automobiles with different physical characteristics and motion types.

2.2 System Components

A key to this concept is immersion in a realistic VR environment with real inputs and cockpits, allowing interaction with the system. The design calls for 3D stereo vision graphics with realistic vehicle environments (delivered via a giant projection screen, or better yet, through a wireless head-mounted display (HMD)), 3D surround sound audio, articulating fans for motion perception enhancement (when the cockpit is not enclosed) and an olfactory generator for realistic smells to increase the sense of realism in our vehicle simulations.

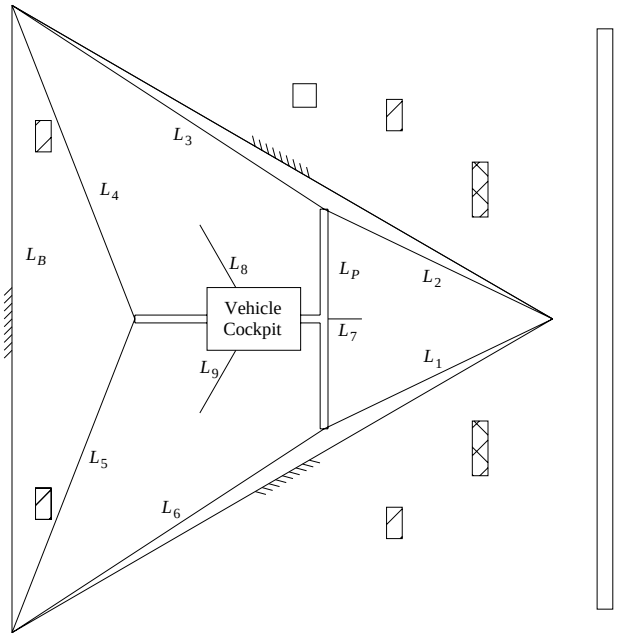

a. Top View.

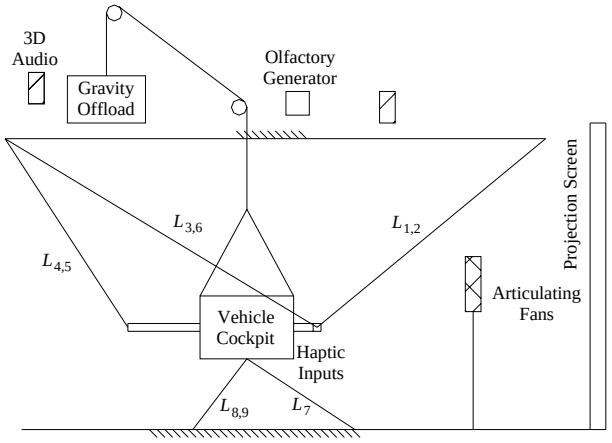

b. Side View.

Figure 2. Whole-Body Haptics Vehicle Simulator System.

From Figure 2, the main system components for VR immersion with whole-body haptics (vehicle simulator motion) are as follows:

- Nine-cable-suspended vehicle simulator
- Real-world cockpit
- Realistic input devices, with haptics where possible, for interaction
- 3D Video projected on a giant screen, in a VR cave, or within a head-mounted display (HMD)
- 3D surround-sound audio
- Articulating fans for simulated breezes in motion

- Olfactory generator for realistic smells
- System for partial gravity offload to allow smaller control motors
- Sensors for inputs and motion feedback including 6-dof tracking technology
- Redundant-cables safety system (not shown)

2.3 Potential Applications

For each of the many vehicles proposed for suspended motion simulation, there are also various applications or missions – many of the following are common to many of the proposed vehicles.

- Research & Development
- Engineering Design and Simulation of Vehicles
- Operator Training
- Safety Research and Training
- Rehabilitation
- Therapy
- Emotional therapy for autistic, mentally-handicapped, and others
- Entertainment
- Recreation for City Dwellers / Access to Experience prior to going out into the real world
- Serious Gaming – including military training/remote control
- High-End Arcades – to make the human player more active

3. VEHICLE SIMULATION SYSTEM KINEMATICS

Figure 3 shows the vehicle simulation system kinematic diagram. This cable-suspended robot is intended to be a versatile, economic, accurate, stiff, safe vehicle simulation tool for various applications as discussed above.

In Figure 3, the fixed base Cartesian coordinate frame is $\{B\}$ and the moving vehicle simulation platform has Cartesian coordinate frame $\{P\}$ fixed to its CG. The active control tensioning motors are mounted to the base frame: two motors each at fixed cable connection points B_1, B_2, and B_3, and one motor each at fixed cable connection points B_4, B_5, and B_6. The cable-connection vertices of the moving platform are P_1, P_2, P_3, and P_4, and point P is the centroid of the moving vehicle platform. In Figure 3, equilateral triangles are assumed for the fixed ceiling base points, the moving platform upper cable-connection points, and the fixed floor base points with sides L_B (shown), L_P (shown), and L_{Bfloor} (not shown), respectively. However, any desired geometry may be used for these important points; the kinematics equations presented in the next section will be identical.

The lengths of the nine active cables are $L_i,\ i=1,2,\cdots,9$. As shown in Figure 3, the upper RoboCrane cables are described as follows: cable L_1 connects P_1 to B_1, cable L_2 connects P_2 to B_1, cable L_3 connects P_2 to B_2, cable L_4 connects P_3 to B_2, cable L_5 connects P_3 to B_3, and cable L_6 connects P_1 to B_3. Also shown in Figure 3, the lower three down-pulling cables are described as follows: cable L_7 connects P_4 to B_4, cable L_8 connects P_4 to B_5, and cable L_9 connects P_4 to B_6.

3.1 VSS Inverse Pose Kinematics Solution

The inverse pose kinematics problem is stated: Given the desired moving vehicle platform pose $\left[{}^{B}_{P}\mathbf{T}\right]$, calculate the nine active cable lengths $L_i,\ i=1,2,\cdots,9$. The solution to this problem may be used as the basis for a pose control scheme, executing both pre-planned trajectories and/or real-time interactive vehicle simulations based on human inputs and a virtual vehicle dynamics model. The VSS inverse pose kinematics solution is straight-forward and poses no computational challenge for real-time implementation: given the moving platform pose, we can easily find the moving platform cable connection points P_1, P_2, P_3, and P_4. Then the inverse pose solution consists simply of calculating the cable lengths using the Euclidean norm of the appropriate vector differences between the various moving and fixed cable connection points. The inverse pose kinematics solution yields a unique closed-form solution.

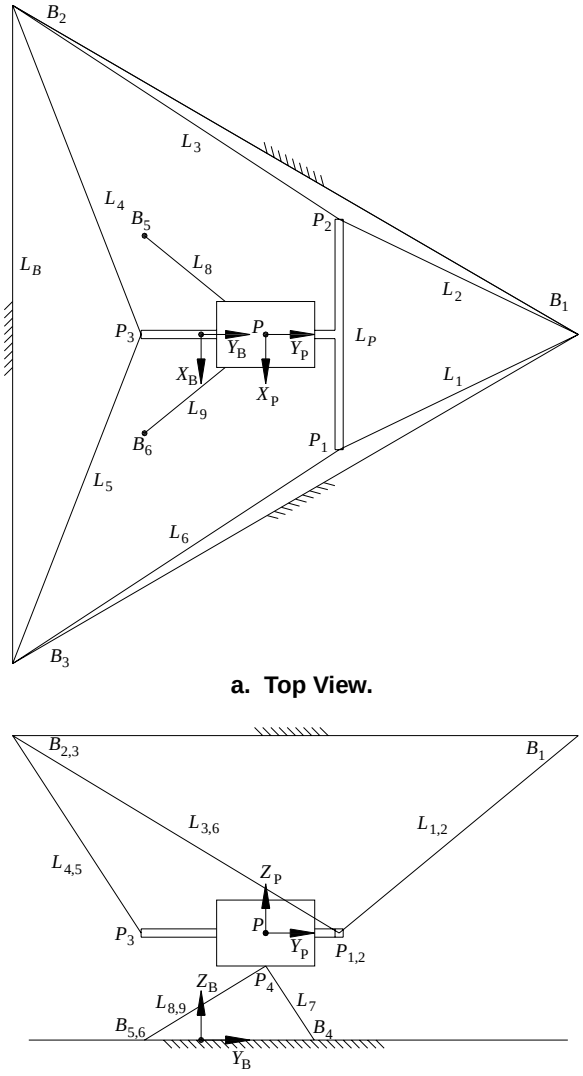

Figure 3. Vehicle Simulation System Kinematic Diagram.

Given $\left[{}^{B}_{P}\mathbf{T}\right]$ we calculate the moving cable connection points P_1, P_2, P_3, and P_4 referenced to the fixed base frame $\{B\}$ using:

$$\left\{{}^{B}\mathbf{P}_i\right\}=\left[{}^{B}_{P}\mathbf{T}\right]\left\{{}^{P}\mathbf{P}_i\right\} \qquad i=1,2,3,4 \qquad (1)$$

Note we must augment each position vector in (1) with a '1' in the fourth row to make the 4x4 matrix multiplication indices work. The

constant relative vectors $\left\{ {}^{P}\mathbf{P}_i \right\}$ are known from platform geometry, the four position vectors to point P_i from the origin of $\{P\}$, expressed in $\{P\}$ coordinates. The resulting vectors $\left\{ {}^{B}\mathbf{P}_i \right\}$ are the position vectors to point P_i from the origin of $\{B\}$, expressed in $\{B\}$ coordinates. Given the four moving cable connection points from (1), we find the nine unknown cable lengths using the following Euclidean norms of the appropriate vector differences between fixed base and moving platform cable-connection points:

$$\begin{aligned} L_1 &= \left\| {}^{B}\mathbf{B}_1 - {}^{B}\mathbf{P}_1 \right\| \quad L_2 = \left\| {}^{B}\mathbf{B}_1 - {}^{B}\mathbf{P}_2 \right\| \quad L_3 = \left\| {}^{B}\mathbf{B}_2 - {}^{B}\mathbf{P}_2 \right\| \\ L_4 &= \left\| {}^{B}\mathbf{B}_2 - {}^{B}\mathbf{P}_3 \right\| \quad L_5 = \left\| {}^{B}\mathbf{B}_3 - {}^{B}\mathbf{P}_3 \right\| \quad L_6 = \left\| {}^{B}\mathbf{B}_3 - {}^{B}\mathbf{P}_1 \right\| \\ L_7 &= \left\| {}^{B}\mathbf{B}_4 - {}^{B}\mathbf{P}_4 \right\| \quad L_8 = \left\| {}^{B}\mathbf{B}_5 - {}^{B}\mathbf{P}_4 \right\| \quad L_9 = \left\| {}^{B}\mathbf{B}_6 - {}^{B}\mathbf{P}_4 \right\| \end{aligned} \tag{2}$$

3.2 VSS Forward Pose Kinematics Solution

The forward pose kinematics solution is required for simulation and sensor-based control of the VSS. The forward pose kinematics problem is stated: Given the nine active cable lengths L_i, $i = 1,2,\cdots,9$, calculate the resulting moving vehicle platform pose $\left[{}^{B}_{P}\mathbf{T} \right]$. Generally for cable-suspended robots, the forward pose kinematics solution is not as straight-forward as the inverse pose kinematics solution. For instance, the 6-cable RoboCrane with the simplified 3-3 Stewart-Gough Platform geometry has a closed-form solution that is quite complicated, yielding 16 possible solutions (generally not all real) by finding the roots of a 16th–order polynomial (Williams, 1992). However, unlike most parallel robot forward pose kinematics problems, there exists a closed-form solution for the Vehicle Simulation System of Figure 3, and the computation requirements are not demanding. There are multiple solutions, but generally the correct solution for the VSS can easily be determined.

The closed-form VSS forward pose kinematics solution is based on finding the intersection of three spheres (four times in succession). At each step, each sphere center and radius is known. The closed-form three-spheres' intersections algorithm is straight-forward and not computationally-intensive (Williams et al., 2004).

The first step in the forward pose kinematics solution is to calculate lower platform cable-connection point P_4 given the lower active cable lengths L_7, L_8, and L_9 using the intersection of three spheres algorithm and knowing the floor-fixed base points. Then moving platform cable-connection points P_1, P_2, and P_3 can be similarly found, by intersecting three known spheres three different times, each time using this P_4 as one of the sphere centers. Referring to a sphere as a vector center point **c** and scalar radius r, (**c**,r), the VSS forward pose kinematics solution is summarized below:

1. P_4 is the intersection of: ($\mathbf{B}_4$,L_7), ($\mathbf{B}_5$,L_8), ($\mathbf{B}_6$,L_9);
2. P_1 is the intersection of: ($\mathbf{P}_4$,l_{P1}), ($\mathbf{B}_1$,L_1), ($\mathbf{B}_3$,L_6);
3. P_2 is the intersection of: ($\mathbf{P}_4$,l_{P2}), ($\mathbf{B}_1$,L_2), ($\mathbf{B}_2$,L_3); and
4. P_3 is the intersection of: ($\mathbf{P}_4$,l_{P3}), ($\mathbf{B}_2$,L_4), ($\mathbf{B}_3$,L_5).

where the three known lengths fixed on the platform are $l_{P1} = \left\| \mathbf{P_1} - \mathbf{P_4} \right\|$, $l_{P2} = \left\| \mathbf{P_2} - \mathbf{P_4} \right\|$, and $l_{P3} = \left\| \mathbf{P_3} - \mathbf{P_4} \right\|$. The detailed solution for the intersection of three spheres is presented in (Williams et al., 2004). That article also presents discussions on imaginary solutions, singularities, and multiple solutions.

Now let us finish the forward pose kinematics solution. Given ${}^{B}\mathbf{P}_i$, we can calculate the orthonormal rotation matrix $\left[{}^{B}_{P}\mathbf{R} \right]$ directly, using the definition that each column of this matrix expresses the X, Y, and Z unit vectors of $\{P\}$ with respect to $\{B\}$ (Craig, 2005). These columns are calculated as follows, from the moving platform geometry.

$${}^{B}\hat{X}_P = \frac{{}^{B}\mathbf{P}_1 - {}^{B}\mathbf{P}_2}{\left\| {}^{B}\mathbf{P}_1 - {}^{B}\mathbf{P}_2 \right\|} \qquad {}^{B}\hat{Y}_P = \frac{{}^{B}\mathbf{P}_5 - {}^{B}\mathbf{P}_3}{\left\| {}^{B}\mathbf{P}_5 - {}^{B}\mathbf{P}_3 \right\|} \qquad {}^{B}\hat{Z}_P = {}^{B}\hat{X}_P \times {}^{B}\hat{Y}_P \tag{3}$$

where ${}^{B}\mathbf{P}_5$ is the midpoint of P_1P_2. Finally, to find the platform control point P where the $\{P\}$ frame is affixed, we use the following vector loop-closure equation:

$${}^{B}\mathbf{P}_P = {}^{B}\mathbf{P}_4 - {}^{B}_{P}\mathbf{R}\,{}^{P}\mathbf{P}_4 \tag{4}$$

Given $\left\{ {}^{B}\mathbf{P}_P \right\}$ and $\left[{}^{B}_{P}\mathbf{R} \right]$, we then have the 4x4 description of pose, $\left[{}^{B}_{P}\mathbf{T} \right]$, as follows(Craig 2005):

$$\left[{}^{B}_{P}\mathbf{T} \right] = \begin{bmatrix} & \left[{}^{B}_{P}\mathbf{R} \right] & & \left\{ {}^{B}\mathbf{P}_P \right\} \\ 0 & 0 & 0 & 1 \end{bmatrix} \tag{5}$$

There are two solutions to the intersection point of three given spheres (Williams et al., 2004). Therefore, the forward pose kinematics problem yields a total of $2^4 = 16$ mathematical solutions since we must repeat the algorithm four times for the VSS. It is generally straight-forward to determine the correct unique solution using logic in the forward pose kinematics solution implementation.

The down-pulling cables allow for a big improvement over the standard RoboCrane: the existence of a straight-forward forward pose kinematics solution, in addition to improved upper cable tensioning.

4. VEHICLE SIMULATION SYSTEM PSEUDOSTATICS

To maintain safe and stable control in all motions, all cable tensions must remain positive at all times. First, gravity will help to ensure that the top six active cables remain in tension, as long as the rotations are not too far from the horizontal nominal orientation. Further, the cable-suspended robot of Figures 2 and 3 is overactuated (three more cables than the minimum number of six cables for a ceiling-mounted RoboCrane and 6-dof operation). This actuation redundancy will be used to attempt to ensure cable tensions for all motions. We develop a pseudostatic model in this section and then apply it in attempt to maintain positive cable tensions using two methods: a pseudoinverse-based actuation redundancy resolution scheme and then a method wherein the cable tensions of the three lower cables are specified and the remaining unknowns calculated without redundancy.

4.1 Equations for Static Equilibrium

This section presents statics modeling for the 9-cable VSS robot. All nine active cables connect in parallel from the fixed base to the moving platform. The 9 active drive cables have variable tensions which must be maintained as positive. For static equilibrium the sum of all active and passive cable tensions plus gravitational loading

acting on the moving platform must equal the resultant wrench exerted on the environment by the robot. For free-space pseudostatic motions, this resultant wrench is zero; when the tool is in contact with the environment, there is no robot motion, but the resultant wrench is non-zero. We envision that the VSS will generally be used only for free-space motions, with zero contact wrench for all motion, so the only external loading on the moving platform will be due to gravity. However, we will include the environment wrench in case it is required in the future for any application. Figure 4 shows the statics free-body diagram for the moving platform where *CG* indicates the center of mass point. The nine active cable tension vectors are $\mathbf{t}_i$, $i = 1, 2, \cdots, 9$. Now we derive the pseudostatics Jacobian matrix based on the force and moment statics equations. This Jacobian matrix is a linear transformation mapping scalar cable tension magnitudes into the Cartesian wrench of the moving platform.

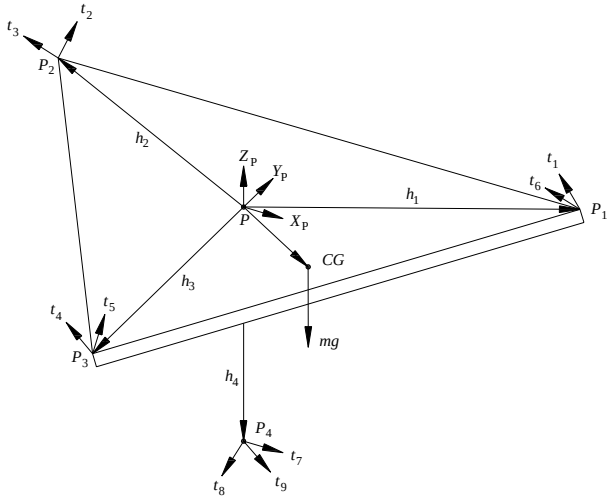

Figure 4. Moving Platform Free-Body Diagram.

The vector translational and rotational equations of static equilibrium are:

$$\sum_{i=1}^{9} \mathbf{t}_i + m\mathbf{g} = \mathbf{F}_R \tag{6}$$

$$\sum_{i=1}^{9} \mathbf{m}_i + {}^B_P\mathbf{R}\,{}^P\mathbf{P}_{CG} \times m\mathbf{g} = \mathbf{M}_R \tag{7}$$

where $\mathbf{t}_i = t_i \hat{\mathbf{L}}_i$ is the vector cable tension applied to the moving platform by the i^{th} active drive cable and (in the positive cable length direction $\hat{\mathbf{L}}_i$ and because $\mathbf{t}_i$ must be in tension; $\hat{\mathbf{L}}_i$ are defined to point from the moving platform to the fixed base); m is the total mass of the moving platform with vehicle cockpit; $\mathbf{g} = \{0 \quad 0 \quad -g\}^T$ is the gravity vector; $\mathbf{m}_i = {}^B_P\mathbf{R}\mathbf{p}_i \times \mathbf{t}_i$ is the moment due to the i^{th} active cable tension ($\mathbf{p}_i$ is the moment arm from the moving platform control point P to the i^{th} active cable connection point, expressed in $\{P\}$ coordinates); ${}^P\mathbf{P}_{CG}$ is the position vector to the moving platform center of mass (*CG*) from the moving platform control point P; and $\mathbf{F}_R$ and $\mathbf{M}_R$ are the vector force and moment (taken together, wrench) exerted on the environment by the moving platform (both zero for free-space motions). Moments are summed about the platform control point P and all vectors must be expressed in a common frame, $\{B\}$ in this paper. From Figure 4, there are only four distinct moment arms for the nine cable tension moments about P, due to the symmetry in design:

$$\begin{aligned} \mathbf{p}_1 &= \mathbf{h}_1 & \mathbf{p}_2 &= \mathbf{h}_2 & \mathbf{p}_3 &= \mathbf{h}_2 \\ \mathbf{p}_4 &= \mathbf{h}_3 & \mathbf{p}_5 &= \mathbf{h}_3 & \mathbf{p}_6 &= \mathbf{h}_1 \\ \mathbf{p}_7 &= \mathbf{h}_4 & \mathbf{p}_8 &= \mathbf{h}_4 & \mathbf{p}_9 &= \mathbf{h}_4 \end{aligned} \tag{8}$$

Substituting these details into (6) and (7) yields:

$$[\mathbf{S}]\{\mathbf{t}\} = \{\mathbf{W}_R - \mathbf{G}\} \tag{9}$$

where $\{\mathbf{t}\} = \{t_1 \quad t_2 \quad \cdots \quad t_9\}^T$ is the vector of active drive cable tension magnitudes, $\{\mathbf{G}\} = \{m\mathbf{g} \quad {}^B_P\mathbf{R}\,{}^P\mathbf{P}_{CG} \times m\mathbf{g}\}^T$ is the gravity loading wrench vector, $\{\mathbf{W}_R\} = \{\mathbf{F}_R \quad \mathbf{M}_R\}^T$ is the external wrench vector exerted on the environment by the vehicle cockpit, and the active statics Jacobian matrix $[\mathbf{S}]$ is:

$$[\mathbf{S}] = \begin{bmatrix} \hat{\mathbf{L}}_1 & \hat{\mathbf{L}}_2 & \cdots & \hat{\mathbf{L}}_9 \\ -\hat{\mathbf{L}}_1 \times {}^B_P\mathbf{R}\mathbf{p}_1 & -\hat{\mathbf{L}}_2 \times {}^B_P\mathbf{R}\mathbf{p}_2 & \cdots & -\hat{\mathbf{L}}_9 \times {}^B_P\mathbf{R}\mathbf{p}_9 \end{bmatrix} \tag{10}$$

One benefit of the active statics Jacobian matrix $[\mathbf{S}]$ is that it may be readily adapted for resolved-rate (inverse velocity) control without additional computations: The inverse Jacobian matrix $\mathbf{M}$ is closely related to the active statics Jacobian matrix of (10): $\mathbf{M} = -\mathbf{S}^T$. We do not present this in the current paper but intend to pursue this as one of our vehicle simulation hardware control modes. Also, this section does not yet incorporate the gravity-offload system of Figure 2.

The statics equations (9) can be used in two ways. Given the active cable tensions $\{\mathbf{t}\}$ and each of the nine cable unit vectors $\hat{\mathbf{L}}_i$ from kinematics analysis, forward statics analysis calculates the external wrench $\{\mathbf{W}_R\}$ applied on the environment by the vehicle cockpit, using (9) directly.

For control and vehicle simulation, the more useful problem is inverse statics analysis: calculate the required active cable tensions $\{\mathbf{t}\}$ given the moving platform mass and the desired external wrench $\{\mathbf{W}_R\}$, plus each $\hat{\mathbf{L}}_i$. This solution may be used for tension optimization control, in attempt to ensure all active cables remain in tension for all pseudostatic motions. We have two algorithms for this, presented in the next subsection.

Note that VSS dynamics may be an important factor in cable tensioning, especially for simulated vehicle motions with high velocities and accelerations. That is, certain dynamic motions of the moving platform will cause higher tensions in some cables and lower tensions in other cables, even slack cables (negative tensions) than that predicted by the pseudostatic model of this section. Therefore, future work into dynamics (e.g. see Williams et al., 2003) is required to complement the pseudostatic approach of this paper.

Now, even for relatively slow pseudostatic robot motions, not all desired configurations and wrenches will be able to exist with only positive active cable tensions. Even for zero applied Cartesian wrench (i.e. only supporting the weight of the moving platform and vehicle

cockpit), our cable tension optimization algorithms presented in the next subsection may fail, especially for large rotations of the moving platform away from the nominal horizontal orientation.

4.2 Maintaining Positive Cable Tensions

This subsection presents two approaches to maintain positive cable tensions on all active cables for all robot motion. Both require actuation redundancy, i.e. more active cables than Cartesian dof. The first approach extends our previously-published algorithm employing active cable tension control with a standard particular/homogeneous solutions optimization method (Williams et al., 2003). That article was for planar cable-suspended robots with one degree of actuation redundancy and the current paper is for spatial motion and three degrees of actuation redundancy (i.e. 9 cables for 6 Cartesian dof). The second approach is simpler: specifying and controlling known cable tensions in the down-pulling cables and calculating the six unknown upper cable tensions via the standard non-redundant matrix inverse. To provide the known tensions in the down-pulling cables, we may either include actual linear springs in line with active cables 7, 8, and 9, converting the tension control problem into an easier length control problem for each of these cables, or it may be done with active tension control without physical springs.

4.2.1 Actuation Redundancy Solution

Since our 9-cable vehicle simulation system has actuation redundancy, (9) is underconstrained (6 equations in the 9 unknown active cable tensions $\{\mathbf{t}\}$) which means that there are three infinities of solutions. To invert (9) (solving the required cable tensions $\{\mathbf{t}\}$ achieve wrench $\{\mathbf{W}_R - \mathbf{G}\}$) we adapt the well-known particular and homogeneous solution from rate control of kinematically-redundant serial manipulators:

$$\{\mathbf{t}\} = [\mathbf{S}]^+ \{\mathbf{W}_R - \mathbf{G}\} + \left([\mathbf{I}_9] - [\mathbf{S}]^+ [\mathbf{S}]\right)\{\mathbf{z}\} \tag{11}$$

The first term of (11), $\{\mathbf{t}\}_p = [\mathbf{S}]^+ \{\mathbf{W}_R - \mathbf{G}\}$, is the particular solution to achieve the desired wrench. The matrix $[\mathbf{S}]^+ = [\mathbf{S}]^T \left([\mathbf{S}][\mathbf{S}]^T\right)^{-1}$ is the 9x6 underconstrained Moore-Penrose pseudoinverse of active statics Jacobian $[\mathbf{S}]$. The second term of (11), $\{\mathbf{t}\}_h = \left([\mathbf{I}_9] - [\mathbf{S}]^+ [\mathbf{S}]\right)\{\mathbf{z}\}$, is the homogeneous solution, projecting any arbitrary vector $\{\mathbf{z}\}$ into the null space of $[\mathbf{S}]$. $[\mathbf{I}_9]$ is the 9x9 identity matrix. Vector $\{\mathbf{z}\}$ should be chosen to ensure positive cable tensions in all nine resulting cables. All possible homogeneous active cable tension solutions $\{\mathbf{t}\}_h$ combine to cause zero wrench on the environment from the vehicle cockpit (the wrench is supplied only by the particular solution).

MATLAB function `lsqnonneg` implements a version of (11). It is the least squares solution (minimum norm solution for underconstrained systems of equations such as (9)) subject to only non-negative values on all solution components. This is a good function to use for cable-suspended robots with the constraint that cables can only exert positive tensions.

The following subsection presents a simpler method in attempt to ensure all positive cable tensions for all motions of the VSS.

4.2.2 Specified Lower Cable Tensions Solution

Generally in the particular solution discussed above, the lower three cable tensions turn out to be impossible, i.e. negative, requiring a pushing up to help resist the weight of the platform and vehicle cockpit. The homogeneous solution may be used in an attempt to correct this problem. However, a simpler approach is to simply specify given positive cable tensions for the three lower cables and then determine the required upper six cable tensions for pseudostatic balance. These cable tensions may be time-varying and different from each other depending on motion requirements. They can be provided by physical springs in line with cables 7, 8, and 9, or they may be achieved through active tension control of these cables. This subsection presents the equations to accomplish this cable tensioning method.

First, partition (9) as follows:

$$[\mathbf{S}_{16}]\{\mathbf{t}_{16}\} + [\mathbf{S}_{79}]\{\mathbf{t}_{79}\} = \{\mathbf{W}_R - \mathbf{G}\} \tag{12}$$

where $[\mathbf{S}_{16}]$ is the first six columns of $[\mathbf{S}]$, $[\mathbf{S}_{79}]$ is the last three columns of $[\mathbf{S}]$, $\{\mathbf{t}_{16}\}$ is the unknown vector of upper cable tensions 1 through 6, and $\{\mathbf{t}_{79}\}$ is the specified vector of cable tensions 7 through 9 (the three down-pulling cables). Then we can solve for the unknowns $\{\mathbf{t}_{16}\}$ using the standard square matrix inverse:

$$\{\mathbf{t}_{16}\} = [\mathbf{S}_{16}]^{-1} \left(\{\mathbf{W}_R - \mathbf{G}\} - [\mathbf{S}_{79}]\{\mathbf{t}_{79}\}\right) \tag{13}$$

(13), combined with the specified values for $\{\mathbf{t}_{79}\}$ form a valid solution to (9) with all positive cable tensions, assuming $\{\mathbf{t}_{79}\}$ were specified to be positive, and the vehicle cockpit orientation does not rotate too far from nominal.

5. EXAMPLES

For all examples in this paper, the following VSS parameters were used. The upper ceiling-mounted fixed-base cable connection points are on the vertices of an equilateral triangle with side 4 *m*. The moving platform cable-connection vertices are on an equilateral triangle of side 1 *m*. The down-pulling cables attach to the lower vehicle cockpit at the triangle centroid, 0.2 m below the plane of the triangle. The lower floor-mounted fixed-based cable connection points on an equilateral triangle of side 1 *m*. The floor-to-ceiling height is 3 *m*. The platform mass is assumed to be 100 *kg* and the platform CG is assumed to be the same as the platform control point *P* (the centroid of the platform equilateral triangle).

5.1 Inverse Pose and Pseudostatics Snapshot Example

Given the desired pose of the moving platform with respect to the base in terms of position vector and *Z-Y-X* Euler angles:

$${}^B\mathbf{X}_T = \begin{Bmatrix} x \\ y \\ z \\ \alpha \\ \beta \\ \gamma \end{Bmatrix} = \begin{Bmatrix} 0.2 \\ 0.6 \\ 1.5 \\ 15 \\ 10 \\ 5 \end{Bmatrix} \text{ (}m\text{ and }deg\text{)}$$

the assignment is to calculate the associated active cable lengths and cable tensions. The associated input homogeneous transformation is calculated:

$$\left[{}^{B}_{P}\mathbf{T}\right] = \begin{bmatrix} 0.9513 & -0.2432 & 0.1897 & 0.2 \\ 0.2549 & 0.9662 & -0.0394 & 0.6 \\ -0.1736 & 0.0858 & 0.9811 & 1.5 \\ 0 & 0 & 0 & 1 \end{bmatrix}$$

The inverse pose kinematics solution (2) yielded the following nine active cable lengths (*m*): L_1 = 2.1224, L_2 = 2.1153, L_3 = 2.8805, L_4 = 3.0514, L_5 = 2.5667, L_6 = 3.0092, L_7 = 1.3142, L_8 = 1.7152, and L_9 = 1.6180. The resulting platform vertices are:

$$\left\{{}^{B}\mathbf{P}_1\right\} = \begin{Bmatrix} 0.6054 \\ 1.0064 \\ 1.4380 \end{Bmatrix}, \quad \left\{{}^{B}\mathbf{P}_2\right\} = \begin{Bmatrix} -0.3458 \\ 0.7515 \\ 1.6116 \end{Bmatrix},$$

$$\left\{{}^{B}\mathbf{P}_3\right\} = \begin{Bmatrix} 0.3404 \\ 0.0422 \\ 1.4504 \end{Bmatrix}, \quad \left\{{}^{B}\mathbf{P}_4\right\} = \begin{Bmatrix} 0.1621 \\ 0.6079 \\ 1.3038 \end{Bmatrix}$$

To hold the VSS in static equilibrium the required cable tensions from the particular solution (the first term of (11)) are given on the left below. Since the lower three cables require negative cable tensions from the particular solution, we cannot use it directly (the bottom cables are required to push to obtain static equilibrium using the least-squares solution approach). Instead, to simplify, specifying a 50 N positive cable tension for each of cables 7, 8, and 9, we obtain all positive cable tensions using (13), given on the right below:

$$\{\mathbf{t}\} = \begin{Bmatrix} 123.10 \\ 122.02 \\ 165.68 \\ 154.91 \\ 207.18 \\ 97.07 \\ -237.14 \\ -143.07 \\ -164.19 \end{Bmatrix} \qquad \{\mathbf{t}\} = \begin{Bmatrix} \mathbf{t}_{16} \\ \mathbf{t}_{79} \end{Bmatrix} = \begin{Bmatrix} 408.00 \\ 439.76 \\ 216.85 \\ 186.81 \\ 381.99 \\ 173.33 \\ 50 \\ 50 \\ 50 \end{Bmatrix}$$

5.2 Forward Pose Check of the Same Snapshot Example

Given the nine active cable lengths (*m*): L_1 = 2.1224, L_2 = 2.1153, L_3 = 2.8805, L_4 = 3.0514, L_5 = 2.5667, L_6 = 3.0092, L_7 = 1.3142, L_8 = 1.7152, and L_9 = 1.6180, the assignment is to calculate the resulting pose of the moving platform with respect to the base, $\left[{}^{B}_{P}\mathbf{T}\right]$. The forward pose kinematics solution yielded the following solution, identical to the input of the inverse pose kinematics problem, as expected (given at the top of this page).

The moving platform cable-connection points were identical to those listed above. The pseudostatic cable tensions are also identical to those listed above. The graphical VSS pose for these identical snapshot examples is shown in Figure 5.

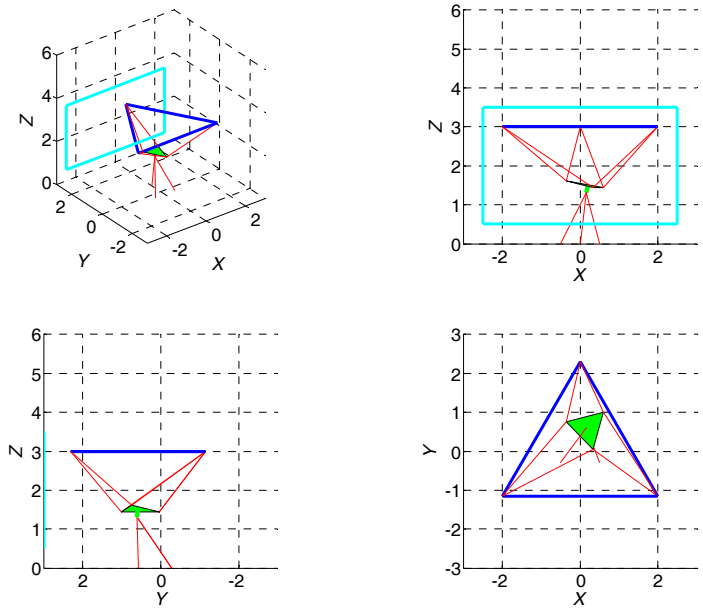

Figure 5. Pose for Snapshot Examples.

5.3 Inverse Pose Kinematics Trajectory Example

Now we present an inverse-pose-based trajectory example wherein we can command general sine waves with independent amplitudes and frequencies on each of the 6 Cartesian motions (3 translations and 3 rotations). Specifically we will request the simulated VSS to move in a sine wave in the *Z* direction with 1 *m* amplitude and 1 *rad*/*s* frequency while simultaneously rotating about the *Z* axis with a sine wave of 30 *deg* amplitude and 2 *rad*/*s* frequency, from an initial pose of:

$${}^{B}\mathbf{X}_T = \begin{Bmatrix} x \\ y \\ z \\ \alpha \\ \beta \\ \gamma \end{Bmatrix} = \begin{Bmatrix} 0 \\ 0 \\ 1.5 \\ 0 \\ 0 \\ 0 \end{Bmatrix}$$

We simulated this motion for 10 *sec*; Figure 6 shows a motion snapshot at *t* = 6.0 *sec*. For this trajectory example, Figure 7a shows the commanded Cartesian pose, Figure 7b shows the required cable lengths as calculated by the inverse pose kinematics solution at each time step, Figure 7c shows the nine active cable tensions calculated via the particular solution component of (11), Figure 7d shows the nine active cable tensions calculated via the complete solution (11) implemented by MATLAB function `lsqnonneg`, and Figure 7e shows the nine active cable tensions calculated by specifying positive cable tensions of 30, 20, and 10 *N* for the lower three cables 7, 8, and 9, respectively, and using (13).

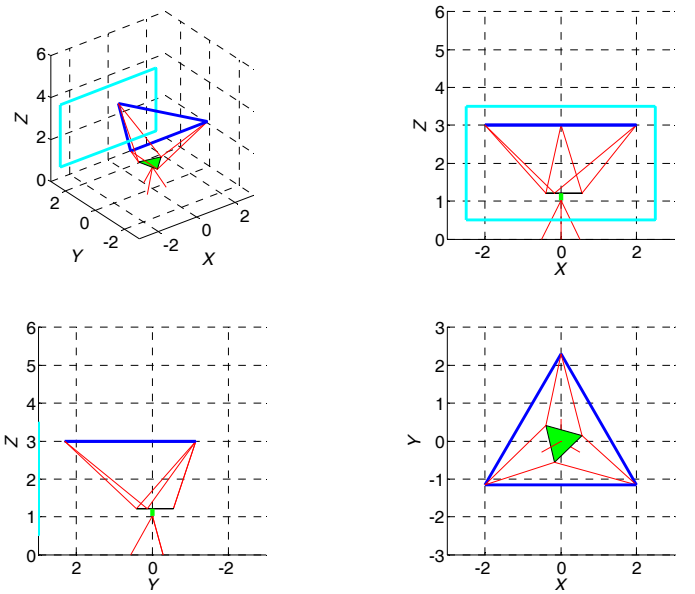

Figure 6. Pose for Trajectory Example at t = 6 *sec.*

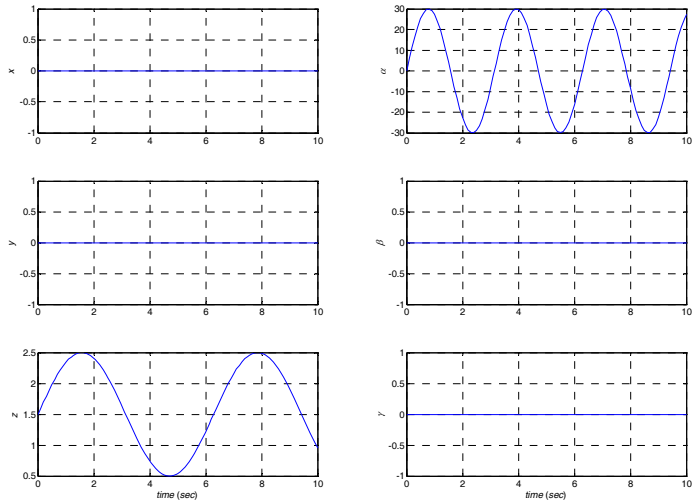

Figure 7a. Commanded Cartesian Pose for Trajectory.

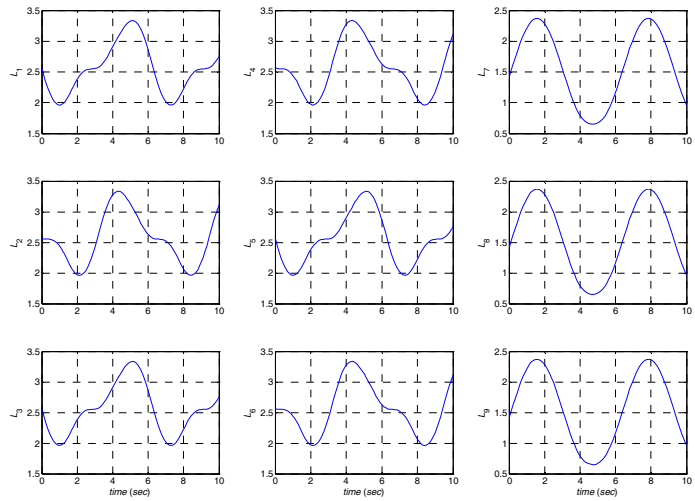

Figure 7b. Required Cable Lengths for Trajectory.

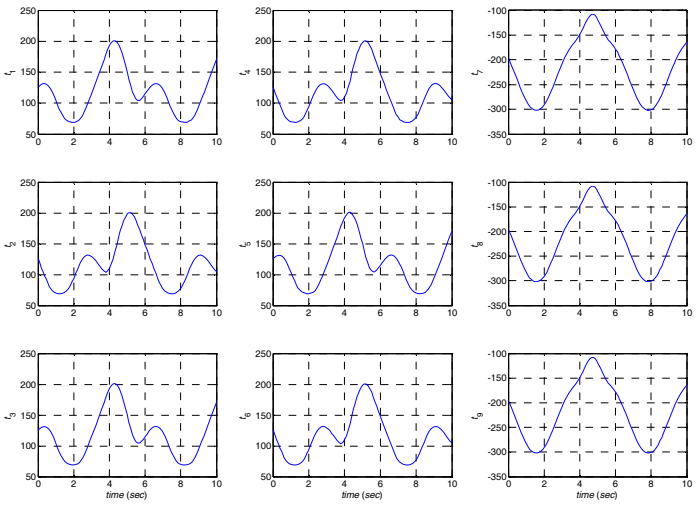

Figure 7c. Particular Solution Tensions for Trajectory.

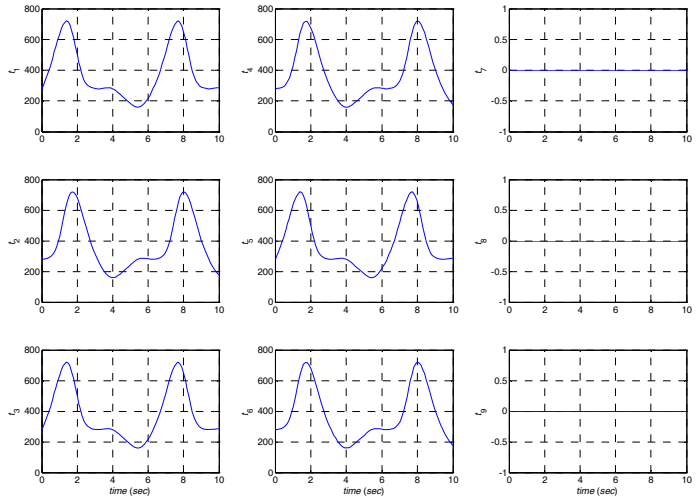

Figure 7d. Isqnonneg Tensions Solution for Trajectory.

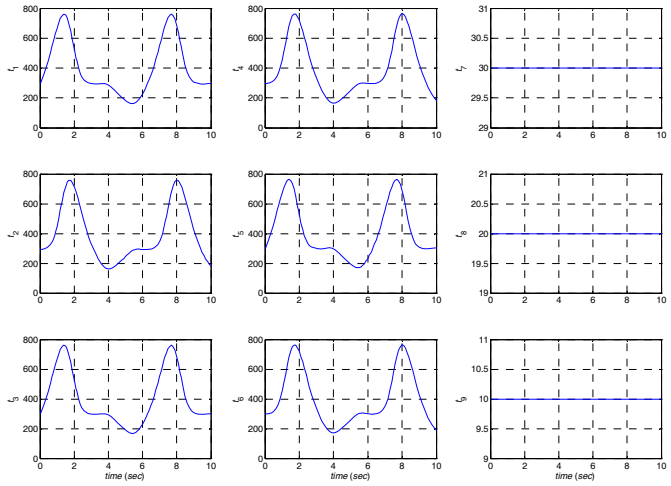

Figure 7e. Tensions with $\{\mathbf{t}_{79}\}$ Specified for Trajectory.

Figure 7a shows the commanded (and, simulated, achieved) Cartesian motions from the initial pose: a sine wave in the *Z* direction with 1 *m* amplitude and 1 *rad*/*s* frequency plus rotating about the *Z* axis with a sine wave of 30 *deg* amplitude and 2 *rad*/*s* frequency. Figure 7b shows the required cable lengths to achieve this motion, calculated from the inverse pose kinematics solutions. Due to the special symmetry in motion (pure vertical translation and only cockpit yaw, no pitch or roll), there is special symmetry in the cable length solutions: cable lengths 1, 3, and 5 are identical, cable lengths 2, 4, and 6 are identical, and cable lengths 7, 8, and 9 are identical, all of which make sense from the arrangement of cables in the VSS.

For this simulated motion, Figure 7c shows the cable tensions calculated by the particular solution of (11) only. These tensions are impossible since the lower three down-pulling cables have negative tensions (cables 7, 8, and 9) and thus they are asked to be up-pushing cables, which is impossible. This is always the case for our specific VSS design. The next two figures present attempts to correct this problem. Figure 7d shows the results of MATLAB function `lsqnonneg` over the commanded trajectory. We see that the lower cable tensions turn out to be zero for all motion (the minimum allowable tension values) and all six upper cables have significantly higher tensions than the (impossible) results of Figure 7c. In Figure 7e we used (13) by enforcing constant positive values for cable tensions 7, 8, and 9 of 30, 20, and 10 *N*, respectively. These results are not greatly different from those of Figure 7d; all upper cable tensions are somewhat greater over the entire simulated motion. In fact, if we specify 0 cable tensions for the lower cables 7, 8, and 9, and use (13), we get identical results to the MATLAB function `lsqnonneg` as shown in Figure 7d.

6. CONCLUSION

This paper presents a concept for a cable-suspended vehicle simulation system. This system is intended to simulate the dynamics of a wide variety of real-world vehicles using VR immersion. 'Driving' from a realistic cockpit of the vehicle to be simulated, with realistic input devices possibly providing force feedback, the system provides motions to the human user designed to mimic real-world motions; this is termed whole-body haptics (the human rides in the cable-suspended cockpit, similar to Stewart-platform flight simulations). Applications include vehicle operator training, vehicle research & development, gaming and entertainment (to enable active participation), plus rehabilitation and therapy.

This Vehicle Simulation System has the potential to improve upon existing Stewart Platform-based flight simulations: the proposed system could be lighter, stiffer, have higher accelerations, have better safety and lower cost, and simulate a larger range of vehicles. This is merely stated as a hypothesis – the current paper does not attempt to prove any of these claims since it only introduces the concept, kinematics and pseudostatics equations, and some simulated motion examples.

Future work plans include design and construction of a human-enabled Vehicle Simulation System prototype including realistic exchangeable cockpits and VR immersion.

REFERENCES

J.S. Albus, R. Bostelman, and N.G. Dagalakis, 1993, "*The NIST ROBOCRANE*", Journal of Robotic Systems, 10(5): 709-724.

I. Bonev, 2003, "The True Origins of Parallel Robots", http://www.parallemic.org/Reviews/Review007.html.

P.D. Campbell, P.L. Swaim, and C.J. Thompson, 1995, "Charlotte Robot Technology for Space and Terrestrial Applications", 25th International Conference on Environmental Systems, San Diego, SAE Article 951520.

K.L. Cappel, 1967, "Motion Simulator," US Patent 3,295,224.

J.J. Craig, 2005, Introduction to Robotics: Mechanics and Control, 3rd Edition, Pearson Prentice Hall, Upper Saddle River, NJ.

V.E. Gough and S.G. Whitehall, 1962, "Universal Tyre Test Machine," Proceedings of the FISITA Ninth International Technical Congress: 117-137.

P. Lafourcade, M. Llibre, and C. Reboulet, 2002, "Design of a Parallel Wire-Driven Manipulator for Wind Tunnels", Proceedings of the Workshop on Parallel Mechanisms and Manipulators, Quebec City, Canada: 187-194.

D. Stewart, 1965-66, "A Platform with Six Degrees of Freedom," Proceedings of the IMechE, 180 Part 1(15): 371-385.

R.L. Williams II, 1992, "Kinematics of an In-Parallel Actuated Manipulator Based on the Stewart Platform Mechanism", NASA Technical Memorandum 107585, NASA Langley Research Center, Hampton, VA, March.

R.L. Williams II, J.S. Albus, and R.V. Bostelman, 2004, "3D Cable-Based Cartesian Metrology System", Journal of Robotic Systems, 21(5): 237-257.

R.L. Williams II, P. Gallina, and J. Vadia, 2003, "Planar Translational Cable-Direct-Driven Robots", Journal of Robotic Systems, 20(3): 107-120.